

Jet Tomography in the Forward Direction at RHIC

G.G. Barnaföldi^{1,2} ^a, P. Lévai¹, G. Papp³, and G. Fai⁴

¹ RMKI KFKI, P.O. Box 49, Budapest 1595, Hungary

² Dept. of Physics of Complex Systems, Eötvös University, Pázmány P. 1/A, Budapest 1117, Hungary

³ Dept. for Theoretical Physics, Eötvös University, Pázmány P. 1/A, Budapest 1117, Hungary

⁴ Center for Nuclear Research, Kent State University, Kent, OH 44242, USA

Received: date / Revised version: date

Abstract. Hadron production at high- p_T displays a strong suppression pattern in a wide rapidity region in heavy ion collisions at RHIC energies. This finding indicates the presence of strong final state effects for both transversally and longitudinally traveling partons, namely induced energy loss. We have developed a perturbative QCD based model to describe hadron production in pp collision, which can be combined with the Glauber–Gribov model to describe hadron production in heavy ion collisions. Investigating $AuAu$ and $CuCu$ collisions at energy $\sqrt{s} = 200$ AGeV at mid-rapidity, we find the opacity of the strongly interacting hot matter to be proportional to the participant nucleon number. Considering forward rapidities, the suppression pattern indicates the formation of a longitudinally contracted dense deconfined zone in central heavy ion collisions. We determine parameters for the initial geometry from the existing data.

PACS. 12.38.Mh Quark-gluon plasma in quantum chromodynamics – 24.85+p Quarks, gluons, and QCD in nuclei and nuclear processes – 25.75-q Relativistic heavy ion collisions

1 Introduction

One of the most interesting challenges in high-energy heavy ion collisions is to extract the properties of the produced hot dense medium. The discovery of strong pion suppression at RHIC energies in $AuAu$ collisions [1,2,3] and its detailed analysis [4,5] was the first milestone along the way to determine the parameters of the central space-time region of heavy ion collision. Applying the so called "jet-tomography" method [6,7,8,9] one can "measure" the averaged density of the color charges in the deconfined region on the basis of the induced energy loss of partons traversing the dense region. Previously we have investigated the induced energy loss for transversally propagating partons [10] analyzing mid-rapidity data at different centralities in $AuAu$ collisions [11,12] and we have determined the opacity parameter of the hot dense matter in the transverse direction. The next level is to perform tomography into the forward (or backward) directions and to extract integrated information about the 3-dimensional structure of the color charge density.

In this paper we display forward tomography in $AuAu$ collisions at RHIC energy. Our aim is to understand the latest BRAHMS result [13] obtained in $AuAu$ collisions, where the measured nuclear modification factor, $R_{AA}(p_T)$, displays similar values at different rapidities ($y = 0$ and $y = 3.2$). The explanation of this requires the understanding of competing nuclear effects, namely shadowing, mul-

tiscattering, induced energy loss, and the qualitative consideration of the geometry of the dense partonic region. On the other hand, these data offer a unique possibility to extract information about the properties of the dense matter in the longitudinal direction in the very early stage of the heavy ion collisions.

Our survey will start with the pp and the dAu data as baseline. At large forward rapidities the indication of increasing suppression has been seen in dAu collisions in pion and charged hadron production [14,15]. The analysis of these data helped us include the appropriate shadowing at high rapidities [16,17]. Thus we are able to determine quantitatively the appropriate energy loss in $AuAu$ collisions, assuming that all final state effects are connected to induced radiative energy loss and the geometry of the dense matter.

We briefly introduce our perturbative QCD improved parton model [10,18] and the description of different nuclear effects. The initial state nuclear shadowing and multiple scattering effects are able to reproduce the π^0 spectrum in dAu collisions [16,19]. The final state radiative parton energy loss is modeled by the GLV-method [6]. We extract the opacity of the dense matter in different centrality regions in $AuAu$ and $CuCu$ collisions at $\sqrt{s} = 200$ AGeV at mid-rapidity. On the basis of the extracted opacity values we perform the forward tomography calculations and investigate existing $AuAu$ data at large forward rapidities.

^a E-mail address: bgergely@rmki.kfki.hu

We discuss the obtained results and connect them to the longitudinal geometry of the dense region. Our analysis is based on the application of radiative energy loss of jets in the mid-rapidity and forward rapidities. The role of other nuclear effects (e.g. possible appearance of scattering energy loss for light quarks [20,21]) will be discussed in a forthcoming paper.

2 Theoretical Description of the Model

The high- p_T inclusive pion spectrum in a heavy ion collision can be calculated in a pQCD-improved parton model. Originally this was developed for nucleon-nucleon collision (basically pp), and extended by a Glauber-type collision geometry and initial state nuclear effects for nucleus-nucleus, AA' collisions as [22,23,24]:

$$\begin{aligned}
E_\pi \frac{d\sigma_\pi^{AA'}}{d^3p} &= \int d^2b d^2r t_A(r) t_{A'}(|\mathbf{b} - \mathbf{r}|) \times \\
&\times \frac{1}{s} \sum_{abc} \int_{vw/z_c}^{1-(1-v)/z_c} \frac{d\hat{v}}{\hat{v}(1-\hat{v})} \int_{vw/\hat{v}z_c}^1 \frac{d\hat{w}}{\hat{w}} \int^1 dz_c \times \\
&\times \int d^2\mathbf{k}_{Ta} \int d^2\mathbf{k}_{Tb} f_{a/A}(x_a, \mathbf{k}_{Ta}, Q^2) f_{b/A'}(x_b, \mathbf{k}_{Tb}, Q^2) \\
&\times \left[\frac{d\hat{\sigma}}{d\hat{v}} \delta(1-\hat{w}) + \frac{\alpha_s(Q_r)}{\pi} K_{ab,c}(\hat{s}, \hat{v}, \hat{w}, Q, Q_r, \tilde{Q}) \right] \times \\
&\times \frac{D_c^\pi(z_c, \tilde{Q}^2)}{\pi z_c^2}. \tag{1}
\end{aligned}$$

Here $t_A(b) = \int dz \rho_A(b, z)$ denotes the nuclear thickness function, and it is normalized as usual: $\int d^2b t_A(b) = A$. For proton and deuteron we use a sharp sphere approximation, while for heavy nuclei the Wood-Saxon formula is applied for the nuclear density distribution, $\rho_A(b, z)$.

In our next-to-leading order (NLO) calculation, $d\hat{\sigma}/d\hat{v}$ represents the Born cross section of the partonic subprocess and $K_{ab,c}(\hat{s}, \hat{v}, \hat{w}, Q, Q_r, Q_f)$ is the corresponding higher order correction term, see Ref.s [22,23,24]. We fix the factorization and renormalization scales and connect them to the momentum of the intermediate jet, $Q = Q_R = (4/3)p_q$ (where $p_q = p_T/z_c$), reproducing pp data with high precision at high p_T [19].

To take into account the transverse momentum distribution, we defined the following 3-dimensional parton distribution function (PDF):

$$f_{a/p}(x_a, \mathbf{k}_{Ta}, Q^2) = f_{a/p}(x_a, Q^2) \cdot g_{a/p}(\mathbf{k}_{Ta}). \tag{2}$$

Here, the function $f_{a/p}(x_a, Q^2)$ represents the standard longitudinal NLO PDF as a function of momentum fraction of the incoming parton, x_a , at the factorization scale Q . In the present calculation we use the MRST(cg) parameterization [25]. The partonic transverse-momentum distribution in 2 dimensions, $g_{a/p}(\mathbf{k}_T)$, is characterized by an "intrinsic k_T " parameter as in Refs. [18,24]. In our phenomenological framework we assumed a Gaussian function [18,26].

Nuclear multiscattering is accounted for through a broadening of the incoming parton's transverse momentum distribution function, namely an increase in the width of the Gaussian:

$$\langle k_T^2 \rangle_{pA} = \langle k_T^2 \rangle_{pp} + C \cdot h_{pA}(b). \tag{3}$$

Here, $\langle k_T^2 \rangle_{pp} = 2.5 \text{ GeV}^2$ is the width of the transverse momentum distribution of partons in pp collisions [18,19], $h_{pA}(b)$ describes the number of *effective* NN collisions at impact parameter b , which impart an average transverse momentum squared C . The effectivity function $h_{pA}(b)$ can be written in terms of the number of collisions suffered by the incoming proton in the target nucleus. In Ref. [18] we have found a limited number of semihard collisions, $3 \leq \nu_m \leq 4$ and the value $C = 0.35 \text{ GeV}^2$.

We take into account the isospin asymmetry by using a linear combination of p and n PDFs. The applied PDFs are also modified inside nuclei by the "shadowing" effect, applying the parametrization of Ref. [27].

The last term in the convolution of eq. (1) is the fragmentation function (FF), $D_c^\pi(z_c, \tilde{Q}^2)$. This gives the probability for parton c to fragment into a pion with momentum fraction z_c at fragmentation scale $\tilde{Q} = (4/3)p_T$. We apply the KKP parameterization [28].

Finally we include jet-quenching as a final state effect. The energy loss of high-energy quarks and gluons traveling through dense colored matter can measure the integrated density of the colored particles. This non-Abelian radiative energy loss, $\Delta E(E, L)$, can be described as a function of parton opacity, (or mean number of jet scatterings), $\bar{n} = L/\lambda$, where L is the interaction length of the jet and λ is the mean free path in non-Abelian dense matter. In "thin plasma" approximation the energy loss to first order is given by the following expression [6]:

$$\begin{aligned}
\Delta E_{GLV}^{(1)} &= \frac{2C_R\alpha_s}{\pi} \frac{EL}{\lambda} \int_0^1 dx \int_0^{k_{max}^2} \frac{d\mathbf{k}_T^2}{\mathbf{k}_T^2} \times \\
&\times \int_0^{q_{max}^2} \frac{d^2\mathbf{q}_T \mu_{eff}^2}{\pi(\mathbf{q}_T^2 + \mu^2)^2} \cdot \frac{2\mathbf{k}_T \cdot \mathbf{q}_T (\mathbf{k} - \mathbf{q})_T^2 L^2}{16x^2 E^2 + (\mathbf{k} - \mathbf{q})_T^4 L^2} \\
&= \frac{C_R\alpha_s}{N(E)} \frac{L^2 \mu^2}{\lambda} \log\left(\frac{E}{\mu}\right). \tag{4}
\end{aligned}$$

Here C_R denotes the color Casimir of the quark or gluon jet, $\mu/\lambda \sim \alpha_s^2 \rho_{part}$ is the transport coefficient of the medium, which is proportional to the parton density, ρ_{part} , and μ denotes the color Debye screening scale. $N(E)$ is an energy dependent factor with asymptotic value 4.

Considering a time-averaged, static plasma, the average energy loss, ΔE , will modify the argument of the FFs:

$$\frac{D_{\pi/c}(z_c, \tilde{Q}^2)}{\pi z_c^2} \longrightarrow \frac{z_c^*}{z_c} \frac{D_{\pi/c}(z_c^*, \tilde{Q}^2)}{\pi z_c^2}. \tag{5}$$

Here $z_c^* = z_c / (1 - \Delta E/p_c)$ is the modified momentum fraction.

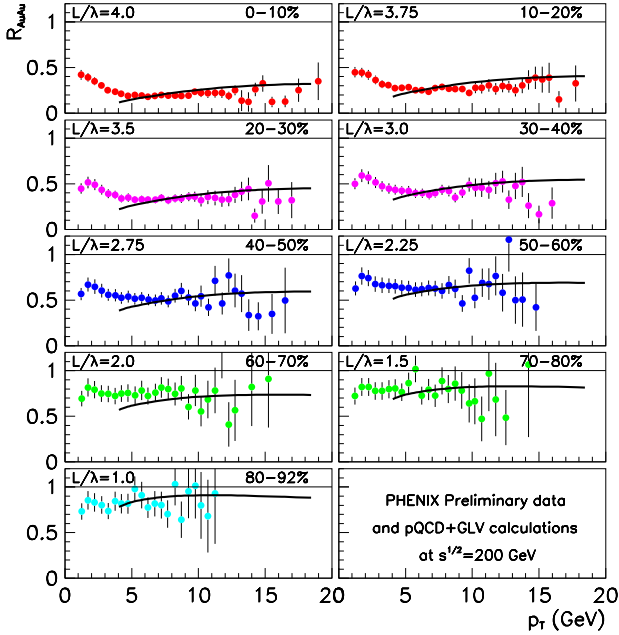


Fig. 1. The nuclear modification factor for π^0 production in $AuAu$ collision, $R_{AuAu}^\pi(p_T)$, at energy $\sqrt{s} = 200$ AGeV at mid-rapidity, measured by PHENIX [29,30]. The solid lines indicate our best fit with the applied opacity parameters, L/λ .

We will present results on hadron productions through the nuclear modification factor, $R_{AA'}(p_T, b)$ defined by

$$R_{AA'}(p_T, b) = \frac{1}{N_{bin}} \cdot \frac{E_\pi d\sigma_\pi^{AA'}(b)/d^3p}{E_\pi d\sigma_\pi^{pp}/d^3p}. \quad (6)$$

Here N_{bin} is the average number of binary collisions, as a function of p_T at different impact parameter ranges.

3 Jet Tomography in Different AA Systems

The opacity parameter, $\bar{n} = L/\lambda$, can be determined by finding the best fit for energy loss and comparing the theoretical results to the data points on the nuclear modification factor. In this section we present our jet tomography results in the mid-rapidity region.

Fig. 1 displays our fit on opacity in $AuAu$ collision at different centralities, using the preliminary data of the PHENIX collaboration on π^0 production at mid-rapidity at $\sqrt{s} = 200$ AGeV energy [29,30]. Experimental data indicate a stronger suppression pattern at $p_T > 4$ GeV/c, thus we read the L/λ values for this region. Here the nuclear modification factor is flat, as Fig. 1 displays. The extracted opacity values are boxed at the top of the panels, together with the centralities. The plotted $R_{AuAu}^\pi(p_T)$ are calculated at the mean values of the opacity, the errors of the fits are approximately ± 0.25 .

The measured suppression pattern in $AuAu$ collision is reproduced well in all centrality bins. In the most central

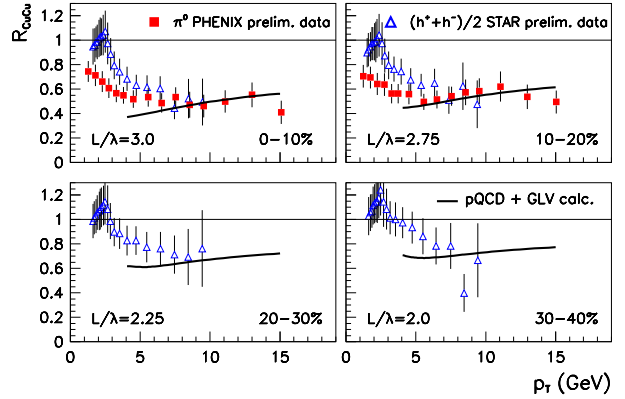


Fig. 2. The nuclear modification factor for pion production in $CuCu$ collision, $R_{CuCu}^\pi(p_T)$, in mid-rapidity at energy $\sqrt{s} = 200$ AGeV. Data are from PHENIX (π^0) [31] and STAR ($\frac{h^+ + h^-}{2}$) [32]. The solid lines indicate our best fit with the applied opacity parameters, L/λ .

(0 – 10%) collisions we have obtained a maximal opacity value, $L/\lambda = 4.0 \pm 0.25$. In the most peripheral collisions (80 – 92%) we have extracted the opacity $L/\lambda = 1.0 \pm 0.25$.

We analyzed the data from $CuCu$ collisions at $\sqrt{s} = 200$ AGeV energy in a similar fashion. Fig. 2 displays the existing data and our calculations. We have found preliminary data on π^0 production from the PHENIX Collaboration in the 0–10% and 10–20% centrality bins [31]. We are able to calculate pion spectra with high precision in our pQCD framework, thus we compare data and theory directly in these two centrality bins. In parallel, STAR data exist on unidentified charged hadrons ($h^\pm := \frac{h^+ + h^-}{2}$) for more centrality bins [32]. In the most central bins we see that the nuclear modification factors overlap for identified pions and unidentified charge hadrons in the very high- p_T region, $p_T > 6 - 8$ GeV/c. (This indicates the restoration of the fragmentation limit for proton and antiproton production in this region, thus the validity of pQCD based calculation for all hadron species — for smaller momenta the contribution from quark coalescence should be included for baryon and antibaryon production [33,34]). Thus, focusing on the highest momentum region, we extracted the opacity values from the STAR data on unidentified charge hadrons and display the data and the theoretical results on Fig. 2 for two more centrality bins, namely for 20 – 30% and 30 – 40%.

Fig. 3 summarizes all mid-rapidity results on opacity for $AuAu$ collisions in the 0 – 92% centrality region (*triangles*) and for $CuCu$ collisions in the 0 – 40% region (*squares*). The opacity parameter, which is connected to the color charge density, is decreasing approximately linearly with increasing centrality, and the slopes of the opacity curves are very similar for $AuAu$ and $CuCu$ collisions. Furthermore, the mid-central (30 – 40%) $AuAu$ collisions are characterized by the same opacity parameter as the most central (0 – 10%) $CuCu$ case. This overlap can be

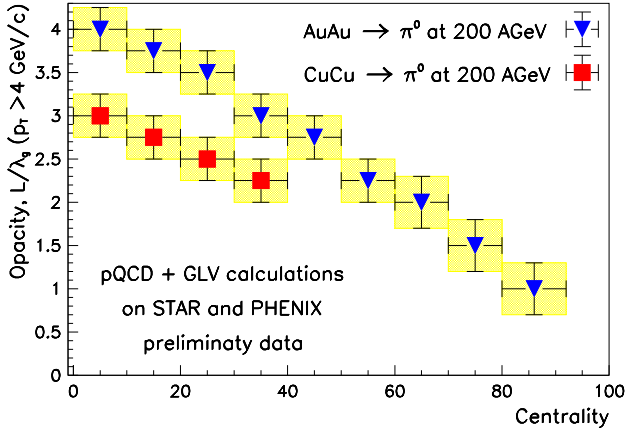


Fig. 3. The centrality dependence of the opacity parameter, L/λ , in $AuAu$ (triangles) and $CuCu$ (squares) collisions at energy $\sqrt{s} = 200$ AGeV.

seen clearly in the measured nuclear modification factors for $AuAu$ and $CuCu$ collisions at different centralities and it has been discussed in Refs. [35,36,37]. This effect may present a real challenge to theoretical models as well as the consequences of any explanation.

Fig. 4 displays the extracted opacity parameters as a function of the participant number, $\langle N_{part} \rangle$, in $AuAu$ collisions (triangles) and $CuCu$ collisions (squares). Here the overlap of the two centrality dependent opacity parameter sets is clearly seen. Fitting the opacity values with a continuous function of the participant number (see solid line on Fig. 4), the following functional form has been found:

$$L/\lambda = (0.62 \pm 0.09) \cdot \langle N_{part} \rangle^{0.33 \pm 0.03}. \quad (7)$$

This fit agrees well with the simple expectation based on geometry, namely $L \propto A^{1/3} \propto N_{part}^{1/3}$ [38].

Assuming constant mean free path (λ) and zero formation time, the above fit validates the idea of a volume-dominated jet energy loss for the whole volume of the hot dense matter. This was assumed in the GLV-method [6], thus our analysis is self-consistent. Combining this result with the expression of the induced energy loss in eq. (4), one can obtain the simple connection, $\epsilon = \Delta E/E \propto N_{part}^{2/3}$. In the forthcoming sessions we will assume the presence of volume-dominated energy losses.

On the other hand, in models which lead to surface-dominated jet-energy loss [39,40,41] or which assume non-zero formation times [42] the above picture is modified drastically. It would be interesting to see the centrality dependence in a repeated analysis with these assumptions and the appropriate plots equivalent to Fig. 3 and Fig. 4. However, this is not our aim, here, in this paper.

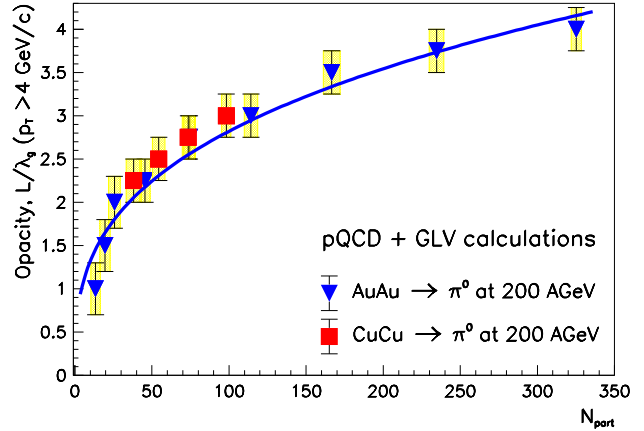


Fig. 4. The opacity parameter, L/λ , as a function of the participant number, $\langle N_{part} \rangle$ in $AuAu$ (triangles) and $CuCu$ (squares) collisions at $\sqrt{s} = 200$ AGeV.

4 Jet Tomography at Large Rapidities

The jet-quenching pattern of the nuclear modification factor is driven by the space and time averaged value of the color-charge density. We are interested in the presence of possible asymmetry between transverse and longitudinal directions seen by the particles produced in different rapidities. Since the produced hot dense matter is characterized by different dynamical behavior in transverse and longitudinal direction, we expect to see this difference during the analysis of available data. Here we analyze hadron production in the forward rapidity region using our theoretical framework and the latest data at RHIC.

In the latest BRAHMS results obtained in the most central $AuAu$ collisions [13,14] the nuclear modification factor, $R_{AA}(p_T)$, displays similar values at different rapidities, namely at $y = 0$ and $y = 3.2$. We expect, that the combination of appropriate geometry of the hot dense partonic region and the competing nuclear effects, namely shadowing, multiscattering, and induced energy loss explain this result. Thus, if we extend our pQCD based calculation and include these latter nuclear effects (which seems to be under control at higher rapidities [16,17]), then the analysis of high rapidity data offers a unique possibility to extract information about the properties of the dense matter in the longitudinal direction in the very early stage of the heavy ion collisions.

The BRAHMS data [13,14] are available in the intermediate- p_T region ($p_T < 4$ GeV/c). We will assume that the suppression factors at different rapidities are approximately the same in the high- p_T region and we will perform our calculations in this manner. This means a suppression factor ~ 5 for $AuAu$ collisions at $\sqrt{s} = 200$ AGeV (seen in the most central collisions in the mid-rapidity [2]) and a suppression factor ~ 3 at $\sqrt{s} = 62.4$ AGeV (see PHENIX data in the most central $AuAu$ collisions [30]).

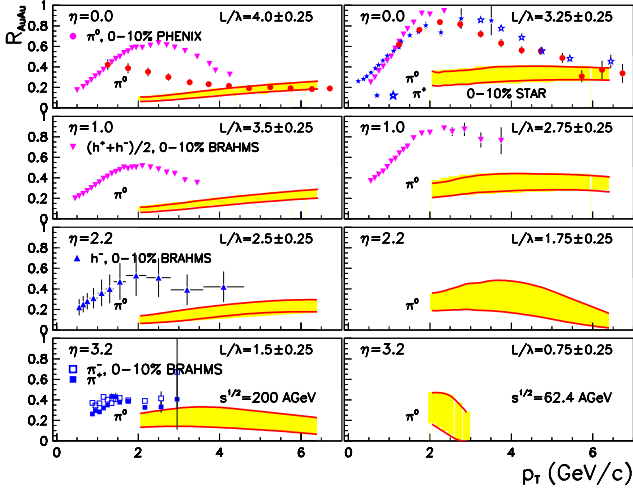


Fig. 5. The pQCD results and the appropriate opacities, L/λ , at different rapidities for pion production in $AuAu$ collisions at $\sqrt{s} = 200$ AGeV (left panels) and 62.4 AGeV (right panels). Data are from BRAHMS [13, 14], PHENIX [2, 30], STAR [32].

Fig. 5 displays our results in the (pseudo)rapidity regions $\eta = 0.0, 1.0, 2.2$ and 3.2 for central $AuAu$ collisions at energies $\sqrt{s} = 200$ AGeV (left panels) and 62.4 AGeV (right panels). Data are from BRAHMS [13, 14] at higher rapidities. The mid-rapidity data are from PHENIX [2, 30] on pion and from STAR [32] on charged hadron production. We display the extracted L/λ opacity values for all rapidities. The extended bands indicate the theoretical uncertainties on the induced energy loss denoted by the errors in the opacity values.

Fig. 6 summarizes the obtained opacity parameters in wide rapidity region for the most central (0–10%) $AuAu$ collisions at $\sqrt{s} = 200$ AGeV and 62.4 AGeV energies. (We have included the opacity parameter from $CuCu$ collisions at $\sqrt{s} = 200$ AGeV.) In the highest energy domain the opacity parameter is decreasing with increasing rapidity from the maximal value of $L/\lambda = 4.0 \pm 0.25$ at mid-rapidity to $L/\lambda = 1.5 \pm 0.25$ at $\eta = 3.2$. Decreasing the collision energy to $\sqrt{s} = 62.4$ AGeV a smaller opacity, $L/\lambda = 3.25 \pm 0.25$ has been extracted at $\eta = 1$. Since no data available at higher rapidities at this energy, we assumed the unmodified suppression factor. This way we have obtained $L/\lambda = 0.75 \pm 0.25$ at $\eta = 3.2$. Fig. 5 can indicate the validity of this assumption. Fig. 6 clearly shows an approximately linear decreasing tendency for the opacity parameter as η is increasing. We have found that at large forward rapidities the interplay between a stronger shadowing and a linearly (in η) decreasing quenching effect is able to maintain a rapidity independent nuclear modification factor.

Fig. 6 displays one more interesting message, what we were looking for. Namely, comparing the extracted opacity values in the mid-rapidity and in the most forward rapidity, one can see a factor of 3 difference at both energies, $\sqrt{s} = 62.4$ AGeV and $\sqrt{s} = 200$ AGeV. According to our assumption the produced hot dense deconfined matter is

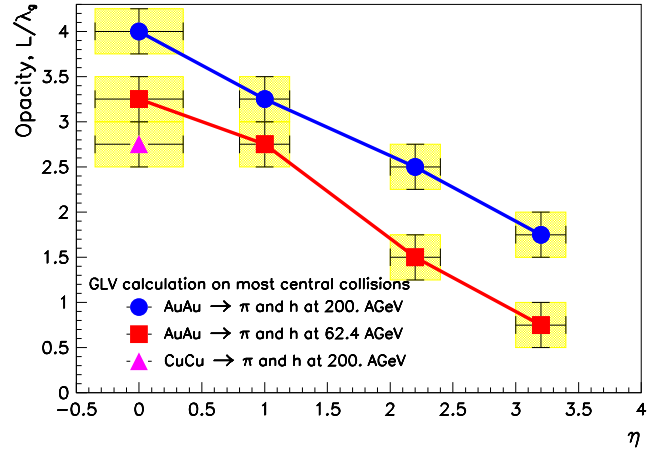


Fig. 6. The opacity parameter L/λ as the function of pseudorapidity (η) for forward pion production in the most central $AuAu$ and $CuCu$ collisions at energies $\sqrt{s} = 62.4, 200$ AGeV, and $CuCu$ collisions at energies $\sqrt{s} = 200$ AGeV.

homogeneous, thus we have a uniform λ value (which may depend on energy but not on geometry). Thus the above result indicates that longitudinally traveling partons see less colored matter than those traveling in the transverse direction. This result can be explained on the basis of pure geometry combined with dynamics.

Fig. 7 displays a schematic picture for the time evolution of the formed hot dense matter and the outgoing jets. Let us characterize the hot matter with the mean free path of $\lambda = 1$ fm. A jet, created in the central region of the collision and producing mostly mid-rapidity hadrons, is traveling transversally through an $L_T \sim 4$ fm length. This jet loses a large portion of its energy and indicates an opacity $L_T/\lambda = 4$. Hadrons in the forward rapidities are produced from forward jets. These jets are moving mostly longitudinally and after passing a (contracted) thin region of the compressed matter (characterized by an effective length of $L_L \sim 1.5$ fm) they reach very quickly the longitudinally expanding surface. Both jet and expansion surface are moving with speed of light, thus the comoving jet does not lose more energy and an opacity $L_L/\lambda = 1.5$ can be extracted at the highest rapidities.

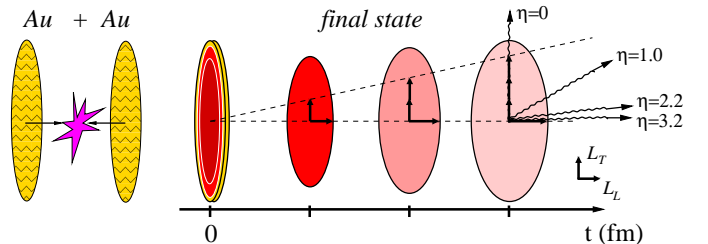


Fig. 7. Time evolution of the quark or gluon jet traveling through the expanding hot dense matter into the transverse and longitudinal direction.

Decreasing the collision energy, the density of the produced hot matter is decreasing and the mean free path is increasing. We do not expect strong modification in the geometry and the comoving dynamics. Thus our results at $\sqrt{s} = 62.4$ AGeV indicate a 25 % increase in the mean free path comparing to the case of $\sqrt{s} = 200$ AGeV.

5 Summary

We have analyzed the measured suppression pattern in *AuAu* and *CuCu* collisions at energy $\sqrt{s} = 200$ AGeV at mid-rapidity. We have found the opacity of the strongly interacting hot matter to be proportional to the participant nucleon number. This result indicates the presence of drastical microscopical mechanisms for energy stopping, which are working in a uniform way at given energy and producing similar energy densities in heavy ion collisions of different nuclei.

Investigating hadron production in forward rapidities, the suppression pattern indicated the formation of a longitudinally contracted dense deconfined zone in the most central heavy ion collisions. We could have determined the initial geometry from the existing data. The decrease of the opacity into the longitudinal direction is explained by the appearance of comoving dynamics.

Our one-hadron tomography can be combined with di-hadron correlation studies [43,44] to obtain more detailed information about the geometry of the hot region. Energy and centrality dependence in *CuCu* collisions could be used to verify our results.

Acknowledgments

One of the authors (GGB) would like thank the support of the Organizers. This work is also supported by Hungarian OTKA T043455, T047050, NK62044, MTA-NSF-OTKA OISE-0435701 and U.S. DE-FG02-86ER40251 grants.

References

1. G. David *et al.* (PHENIX Coll.), Nucl. Phys. **A698** (2002) 227.
2. V. Greene *et al.* (PHENIX Coll.), Nucl. Phys. **A774** (2006) 93.
3. J. Dunlop *et al.* (STAR Coll.), Nucl. Phys. **A774** (2006) 139.
4. P. Lévai *et al.* Nucl. Phys. **A698** (2002) 631.
5. I. Vitev and M. Gyulassy, Phys. Rev. Lett. **89** (2002) 252301.
6. M. Gyulassy, P. Lévai, I. Vitev, Phys. Rev. Lett. **85** (2000) 5535; Nucl. Phys. **B571** (2000) 197; **B594** (2001) 371.
7. B.G. Zakharov, JETP Lett. **63** (1996) 952; **64** (1996) 781; **65** (1997) 615; **70** (1999) 176; **73** (2001) 49; **80** (2004) 617. Phys. Atom. Nucl. **61** (1998) 838.
8. R. Baier, Yu.L. Dokshitzer, A.H. Mueller, S. Peigne, D. Schiff, Nucl. Phys. **B483** (1997) 291; **B484** (1997) 265; **B531** (1998) 403.
9. U.A. Wiedemann, Nucl. Phys. **B582** (2000) 409; Nucl. Phys. **B588** (2000) 303; Nucl. Phys. **A690** (2001) 731.
10. G.G. Barnaföldi *et al.*, Eur. Phys. J. **C33** (2004) S609.
11. D. d’Enterria *et al.* (PHENIX Coll.), Nucl. Phys. **A715** (2003) 749.
12. S.S. Adler *et al.* (PHENIX Coll.), Phys. Rev. Lett. **91** (2003) 072301.
13. P. Staszal *et al.* (BRAHMS Coll.), Nucl. Phys. **A774** (2006) 77.
14. D. Röhrich *et al.* (BRAHMS Coll.), Nucl. Phys. **A774** (2006) 297.
15. I. Arsene *et al.* (BRAHMS Coll.), Phys. Rev. Lett. **93** (2004) 242303; Z. Yin *et al.* (BRAHMS Coll.), J. Phys. **G30** (2004) S983; Z. Yin for the BRAHMS Coll., Acta Phys Hung. **A22** (2005) 309.
16. G.G. Barnaföldi *et al.*, J. Phys. **G30** (2004) S1125.
17. G.G. Barnaföldi *et al.*, Nucl. Phys. **A774** (2006) 801.
18. Y. Zhang *et al.*, Phys. Rev. **C65** (2002) 034903.
19. P. Lévai *et al.*, nucl-th/0306019.
20. M. Djordjevic, M. Gyulassy, S. Wicks, Eur. Phys. J. **C43** (2005) 135.
21. A.Adil, M. Gyulassy, W.A. Horowitz, S. Wicks, nucl-th/0606010.
22. F. Aversa, P. Chiappetta, M. Greco, and J.Ph. Guillet, Nucl. Phys. **B327** (1989) 105.
23. P. Aurenche, M. Fontannaz, J.Ph. Guillet, B. Kniehl, E. Pilon, and M. Werlen, Eur. Phys. J. C **9** (1999) 107; P. Aurenche, M. Fontannaz, J.Ph. Guillet, B. Kniehl, and M. Werlen, Eur. Phys. J. C **13** (2001) 347.
24. G. Papp *et al.*, hep-ph/0212249.
25. A.D. Martin *et al.*, Eur. Phys. Jour. **C23** (2003) 73.
26. G.G. Barnaföldi *et al.*, Heavy Ion Phys. **18** (2003) 79.
27. S.J. Li and X.N. Wang, Phys. Lett. **B527** (2002) 85.
28. B.A. Kniehl, G. Kramer, and B. Pötter, Nucl. Phys. **B597** (2001) 337.
29. B.A. Cole, Nucl. Phys. **A774** (2006) 225.
30. H. Büsching for the PHENIX Coll., Talk on the Hot Quark’06 Conference. See this Proceedings.
31. C. Klein-Bösing for the PHENIX Coll., Proceedings of the 22nd Winter Workshop on Nuclear Dynamics, La Jolla, California, USA, 2006. To appear in Acta Phys. Hung. **A** (nucl-ex/0606013).
32. J. Dunlop for the STAR Coll., Talk on the Quark Matter’05 Conference, 2005, Budapest, Hungary.
33. V. Greco, C.M. Ko, P. Lévai, Phys. Rev. Lett. **90**, 202302 (2003); Phys. Rev. **C68**, 034904 (2003).
34. R.J. Fries, B. Müller, C. Nonaka, S. Bass, Phys. Rev. Lett. **90**, 202303 (2003); Phys. Rev. **C68**, 044902 (2003).
35. S.S. Adler *et al.* (PHENIX Coll.), Phys. Rev. Lett. **91** (2003) 072301;
36. H. Büsching *et al.* (PHENIX Coll.), Nucl. Phys. **A774** (2006) 103.
37. B. Alver *et al.* (PHOBOS Coll.), Phys. Rev. Lett. **96** (2006) 212301;
38. I. Vitev, hep-ph/0511237, To appear in Acta Phys. Hung. (2006).
39. K.J. Eskola, H. Honkanen, C.A. Salgado, U.A. Wiedemann, Nucl. Phys. **A747** (2005) 511.
40. A. Dainese, C. Loizides, G. Paic, Eur. Phys. J. **C38** (2005) 461.
41. V. Pantuev, hep-ph/0506095.
42. S. Peigne, P.-B. Gossiaux, T. Gousset, JHEP 0604 (2006) 011.
43. S.S. Adler *et al.* (PHENIX Coll.), Phys. Rev. Lett. **96** (2006) 222301; hep-ex/0605039.
44. P. Lévai, G. Fai, G. Papp, Phys. Lett. **B634** (2006) 383.